Journal of Solid Mechanics Vol. 6, No. 2 (2014) pp. 194-207

In-plane Band Gaps in a Periodic Plate with Piezoelectric Patches

H.J. Xiang*, Z.B. Cheng, Z.F. Shi, X.Y. Yu

School of Civil Engineering, Beijing Jiaotong University, Beijing, 100044, China

Received 5 March 2014; accepted 4 May 2014

ABSTRACT

A plate periodically bonded with piezoelectric patches on its surfaces is considered. The differential quadrature element method is used to solve the wave motion equation for the two-dimensional periodic structure. The method is very simple and easy to implement. Based on the method, band structures for in-plane wave propagating in the periodic piezoelectric plate are studied, from which the frequency band gap is then obtained. Parametric studies are also performed to highlight geometrical and physical parameters on the band gaps. It is found that the thickness of the piezoelectric patches have no effect on the upper bound frequency of the band gap. Physical mechanism is explained for the phenomena. Dynamic simulations are finally conducted to show how the band gap works for a finite quasi-periodic plate. Numerical results show that the vibration in periodic plates can be dramatically attenuated when the exciting frequency falls into the band gap.

Keywords: Band gap; Piezoelectric; Differential quadrature element method; Periodic materials; Plate

1 INTRODUCTION

PERIODIC structures or materials, whose elastic coefficients or geometrical shapes vary periodically in space, have received considered attention in recent years. The interest in these materials arises mainly from the unique character of having frequency regions, known as absolute band gaps, over which there can be no propagation of elastic waves whatever their polarization and wave vector [1]. The unique character gives periodic structures numerous potential engineering applications, such as noise suppression and the control or isolation of vibrations [2, 3]. Kushwaha and his co-workers firstly conducted the full band-structure calculations for periodic elastic composite materials and introduced the rudimentary idea of 'band-gap engineering' [3, 4]. Liu, Zhang [5] proposed the so-called ‘local resonant’ phononic crystal, which opened a new field for low-frequency and limited size periodic structures. Recently, Shi and his co-workers fabricated periodic foundations to reduce the effect of earthquake waves on structures [6-9]. It is found that the band gap in periodic foundations can be designed in a low frequency region (<20Hz), which lends a new insight into seismic isolation in civil engineering. In addition to their ability to block wave, the periodic structures can prove particularly useful for applications requiring a spatial confinement of acoustic waves and can hence be used as acoustic filters or very efficient waveguides [10].

At the same time, the use of elastic waves in piezoelectric structures is important in a variety of applications, including physical, chemical, and biological sensors. In addition, the piezoelectricity makes it possible to generate and detect waves within composite materials. As an example, this property can be used in piezocomposite acoustic

* Corresponding author. Tel.: +86 10 51684948.
E-mail address: hjxiang@bjtu.edu.cn (H.J. Xiang).

transducers [11]. Recently, attentions have also been paid to wave propagation in periodic structures with piezoelectric materials [12, 13]. Wu, Hsu [14] analyzed the phononic band structure of bulk and surface waves in a two-dimensional periodic structure consisting of an array of piezoelectric cylinders in an isotropic background material based on the plane wave expansion method. Zou, Chen [15] presented detailed calculations of the dispersion relations of waves propagating in two-dimensional piezoelectric composite structures consisting of rectangular piezoelectric ceramic placed periodically in an epoxy substrate with different polarized directions of piezoelectric ceramic for different phononic structures.

There are two main types of using piezoelectric materials in fabricating periodic structures. One is to embed the piezoelectric materials in a substrate. Another type is to bond the piezoelectric materials on the surfaces of a structure. The former one has been studied in the previous studies. The purpose of this paper is to investigate the later one, i.e., a plate periodically bonded with piezoelectric patches. The governing equations for in-plane wave propagation in the plate are presented in Section 2.1. Due to its efficiency, the differential quadrature element method (DQEM) is introduced and used to solve the equations in Sections 2.2 and 2.3. The method had been successfully extended to analyze periodic beams our previous works [16, 17]. However, no publications are concerned with the dispersion analysis of two- or three-dimensional periodic structure using the DQEM. This paper is to further develop the two-dimensional DQEM for dispersion analysis of periodic plates. In Section 3, the band structure for wave propagation in the periodic plates is studied and parametric studies are conducted to show the influences of the physical and geometrical parameters on the band gaps. Numerical simulations are also conducted on the harmonic analysis and the transient analysis to show the effect of band gaps on a finite quasi-periodic plate in Section 4. Finally, some conclusions are given in Section 5.

2 NUMERICAL FORMULATIONS

2.1 Governing equations

As shown in Fig.1(a), some piezoelectric patches of $l_{px} \times l_{py}$ are periodically boned on an infinite homogeneous plate. The center-to-center distance between two adjacent patches is l_{mx} and l_{my} in *x*- and *y*-directions. The distances l_{mx} and l_{my} are the so-called lattice constants [18]. The thicknesses of the hosted plate and the piezoelectric patches are h_m and h_p, respectively. The periodicity of the structure makes it possible to obtain the frequency band gap by studying one periodic unit or Wigner-Seitz cell [16-18] as shown in Fig.1(b).

Let *u* and *v* be the displacements in *x*- and *y*- directions, respectively. Considering an elastic wave with propagation in the plane, the governing dynamic equilibrium equation is:

$$\frac{\partial T_x}{\partial x}+\frac{\partial T_{xy}}{\partial y}=\rho\frac{\partial^2 u}{\partial t^2},\ \frac{\partial T_{xy}}{\partial x}+\frac{\partial T_y}{\partial y}=\rho\frac{\partial^2 v}{\partial t^2} \tag{1}$$

where ρ is the density per area and *t* the time. The stress resultants (T_x ,T_y ,T_{xy}) can be computed by integrating the stress components (σ_x , σ_y , τ_{xy}) over the thickness of the cell as:

$$(T_x, T_y, T_{xy}) = \int (\sigma_x, \sigma_y, \tau_{xy})dz \tag{2}$$

The strains are related to the displacements by

$$\varepsilon_x = \frac{\partial u}{\partial x}, \varepsilon_y = \frac{\partial v}{\partial y}, \varepsilon_{xy} = \frac{1}{2}(\frac{\partial u}{\partial y}+\frac{\partial v}{\partial x}) \tag{3}$$

where ε_x , ε_y , ε_{xy} are the normal strain in *x*- and *y*-directions and the shearing strain, respectively.

For the elastic plate, the linear constitutive equations can be expressed as:

$$\sigma_x = \frac{Y_m}{1-(\mu_m)^2}(\varepsilon_x + \mu_m \varepsilon_y), \sigma_y = \frac{Y_m}{1-(\mu_m)^2}(\varepsilon_y + \mu_m \varepsilon_x), \tau_{xy} = G_m \varepsilon_{xy} \tag{4}$$

where Y_m, G_m, μ_m are Young's modulus, shear modulus and Poisson ratio, respectively. For the piezoelectric patches, the linear constitutive equations are

$$\begin{aligned} &\varepsilon_x = S_{11}\sigma_x + S_{12}\sigma_y + d_{31}E_z,\ \varepsilon_y = S_{12}\sigma_x + S_{11}\sigma_y + d_{31}E_z, \\ &\varepsilon_{xy} = 2(S_{11}-S_{12})\tau_{xy},\ D_z = d_{31}\sigma_x + d_{31}\sigma_y + \in_{33} E_z. \end{aligned} \tag{5}$$

where E_z and D_z are the electric field intensity and electric displacement. S_{ij}, d_{31} and $\in_{33}$ are elastic compliance matrix of the piezoelectric material, piezoelectric constant matrix and dielectric constant matrix, respectively. Two cases are considered: open-circuit and closed-circuit. If the piezoelectric patches are very thin, we can take the electric displacement as zero for the case of open-circuit ($D_z = 0$). By solving Eq. (5), the stresses are then written as:

$$\sigma_x = \frac{Y_p}{1-(\mu_p)^2}(\varepsilon_x + \mu_p \varepsilon_y), \sigma_y = \frac{Y_p}{1-(\mu_p)^2}(\varepsilon_y + \mu_p \varepsilon_x), \tau_{xy} = G_p \varepsilon_{xy} \tag{6}$$

where $Y_p = 1/(S_{11}-S_d)$, $G_p = 0.5/(S_{11}-S_{12})$, $\mu_p = -(S_{12}-S_d)/(S_{11}-S_d)$ and $S_d = d_{31}^2 / \in_{33}$.

Substituting Eq. (3) into Eqs. (4) and (6) and keeping Eq. (2) in mind, we have

$$T_x = C_a \frac{\partial u}{\partial x} + C_b \frac{\partial v}{\partial y},\ T_y = C_b \frac{\partial u}{\partial x} + C_a \frac{\partial v}{\partial y},\ T_{xy} = C_c\left(\frac{\partial u}{\partial y} + \frac{\partial v}{\partial x}\right) \tag{7}$$

and then substituting Eq. (7) into Eq. (1), we can get the dynamic equilibrium equations as follows:

$$C_a \frac{\partial^2 u}{\partial x^2} + (C_b + C_c)\frac{\partial^2 v}{\partial x\,\partial y} + C_c \frac{\partial^2 u}{\partial y^2} = C_d \frac{\partial^2 u}{\partial t^2},\ C_a \frac{\partial^2 v}{\partial y^2} + (C_b + C_c)\frac{\partial^2 u}{\partial x\,\partial y} + C_c \frac{\partial^2 v}{\partial x^2} = C_d \frac{\partial^2 v}{\partial t^2} \tag{8}$$

where the coefficients C_a, C_b, C_c and C_d are listed in Appendix A. The dynamic Eq. (8) can be easily transformed into frequency space as follows:

$$C_a \frac{\partial^2 u}{\partial x^2} + (C_b + C_c)\frac{\partial^2 v}{\partial x\,\partial y} + C_c \frac{\partial^2 u}{\partial y^2} = -C_d \omega^2 u,\ C_a \frac{\partial^2 v}{\partial y^2} + (C_b + C_c)\frac{\partial^2 u}{\partial x\,\partial y} + C_c \frac{\partial^2 v}{\partial x^2} = -C_d \omega^2 v \tag{9}$$

By taking $(u, v) = (u, v)e^{-i\omega t}$ where ω is the angular frequency. For simplicity, we don't distinguish the displacement and its amplitude.

For the case of closed-circuit, if an external voltage V is applied on the piezoelectric patches, the electric field intensity is a constant, i.e., $E_z = V / h_p$. Substituting Eqs. (2) and (5) into Eq. (1), we can find that the dynamic equilibrium equations will be independent of E_z. In other words, the dynamic equilibrium equations will be the same as Eqs. (8)-(9), but the coefficient $S_d = 0$.

Due to the periodicity of the structure, the displacement and stress resultants must satisfy the following periodic boundary conditions according to the Block-Floquet theorem [16-18]

$$u^R = u^L e^{ik_x l_{mx}}, v^R = v^L e^{ik_x l_{mx}}, T_x^R = T_x^L e^{ik_x l_{mx}}, T_{xy}^R = T_{xy}^L e^{ik_x l_{mx}} \tag{10}$$

Between left and right boundaries of the cell, and

$$u^T = u^B e^{ik_y l_{my}}, v^T = v^B e^{ik_y l_{my}}, T_y^T = T_y^B e^{ik_y l_{my}}, T_{xy}^T = T_{xy}^B e^{ik_y l_{my}} \tag{11}$$

Between bottom and top boundaries of the cell. k_x and k_y are the wave number in x- and y-directions,respectively. The superscripts "R", "L", "T" and "B" denote the right, left, top and bottom boundaries, respectively. So u^R and v^R, for example, denote the displacements on the right boundary, which have been shown in Fig.2.

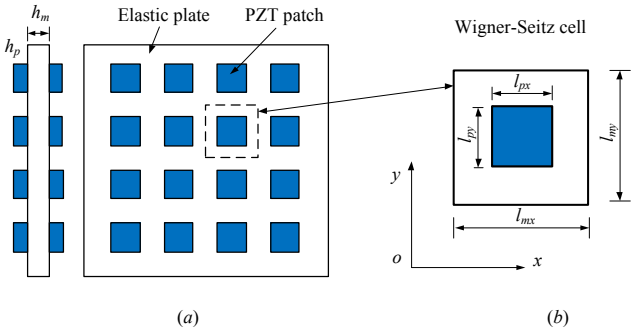

Fig. 1
(a) Configuration of a homogeneous plate with externally periodically bonded piezoelectric patches, (b) The Wigner-Seitz cell.

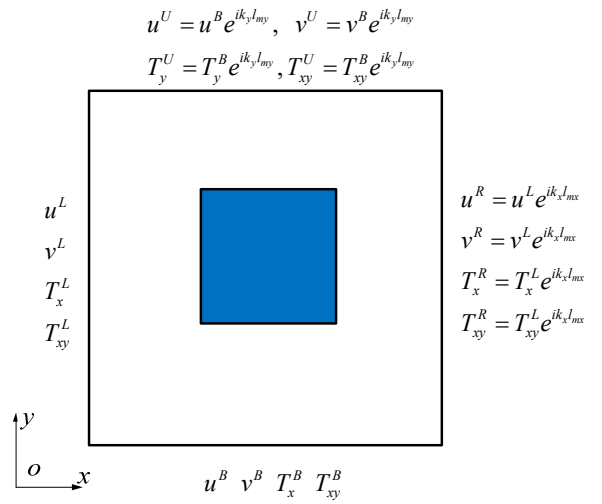

Fig. 2
Periodic boundary conditions.

2.2 Solution method

The differential quadrature element method (DQEM) is a numerical technique for initial or boundary problems, which combines the decomposition process and differential quadrature method [19-22]. The method is adopted to solve Eqs. (9)-(11). The whole solution domain, i.e., the unit cell, is divided into nine elements (or sub-domains) according to the material properties as shown in Fig. 3(a). Let L_x and L_y be the length of the element in x- and y-directions, respectively. As shown in Fig. 3(b), an arbitrary rectangle element is transformed onto a normalized computational domain $[0,1]\times[0,1]$ by the following invertible transformation

$$\xi = \frac{x - x_1}{L_x}, \eta = \frac{y - y_1}{L_y} \tag{12}$$

where ξ and η are the local coordination in the normalized computational domain. (x_1, y_1) is the point at the lower left corner of the element. The governing equations for element n can be expressed in terms of ξ and η

$$\frac{C_a}{\left(L_x\right)^2}\frac{\partial^2 u}{\partial \xi^2}+\frac{C_b+C_c}{L_x L_y}\frac{\partial^2 v}{\partial \xi \partial \eta}+\frac{C_c}{\left(L_y\right)^2}\frac{\partial^2 u}{\partial \eta^2}=-C_d\omega^2 u \tag{13}$$

$$\frac{C_a}{\left(L_y\right)^2}\frac{\partial^2 v}{\partial \eta^2}+\frac{C_b+C_c}{L_x L_y}\frac{\partial^2 u}{\partial \xi \partial \eta}+\frac{C_c}{\left(L_x\right)^2}\frac{\partial^2 v}{\partial \xi^2}=-C_d\omega^2 v \tag{14}$$

and the stress resultants can be rewritten as:

$$T_x=\frac{C_a}{L_x}\frac{\partial u}{\partial \xi}+\frac{C_b}{L_y}\frac{\partial v}{\partial \eta},T_y=\frac{C_a}{L_y}\frac{\partial v}{\partial \eta}+\frac{C_b}{L_x}\frac{\partial u}{\partial \xi},T_{xy}=\frac{C_c}{L_y}\frac{\partial u}{\partial \eta}+\frac{C_c}{L_x}\frac{\partial v}{\partial \xi} \tag{15}$$

The element is further divided into $N_x \times N_y$ grid points in both directions and the Gauss-Lobatto-Chebyshev pattern [23] is used to generate the sampling points

$$\xi_i=\frac{1}{2}\left(1-\cos\frac{(i-1)\pi}{(N_x-1)}\right),\ \eta_j=\frac{1}{2}\left(1-\cos\frac{(j-1)\pi}{(N_y-1)}\right) \tag{16}$$

where $i = 1, 2, \ldots, N_x$ and $j = 1, 2, \ldots, N_y$. The fundamental idea behind the DQEM is to approximate an unknown function and its derivative at any discrete point as the linear weighted sums of its values at all of the discrete points chosen in the element. The functions u, v and their derivatives with respect to ξ or η are approximated by:

$$\{u,v\}=\sum_{i=1}^{N_x}\sum_{j=1}^{N_y} l_i(\xi)l_j(\eta)\{u_{ij},v_{ij}\} \tag{17}$$

$$\frac{\partial^2}{\partial \xi^2}\{u,v\}\Big|_{\xi=\xi_i,\eta=\eta_j}=\sum_{k=1}^{N_x}A_{ik}^{(2)}\{u_{kj},v_{kj}\} \tag{18}$$

$$\frac{\partial^2}{\partial \eta^2}\{u,v\}\Big|_{\xi=\xi_i,\eta=\eta_j}=\sum_{m=1}^{N_y}\bar{A}_{jm}^{(2)}\{u_{im},v_{im}\} \tag{19}$$

$$\frac{\partial^2}{\partial \xi \partial \eta}\{u,v\}\Big|_{\xi=\xi_i,\eta=\eta_j}=\sum_{k=1}^{N_x}\sum_{m=1}^{N_y}A_{ik}^{(1)}\bar{A}_{jm}^{(1)}\{u_{km},v_{km}\} \tag{20}$$

where u_{ij}^n and v_{ij}^n are the displacements at point (ξ_i,η_j), $l_i(\xi)$ and $l_j(\eta)$ are the Lagrange interpolation polynomials, and $A_{ij}^{(r)}$ and $\bar{A}_{ij}^{(r)}$ are the weighting coefficients for the r-th order partial derivatives of displacements with respect to the local coordinates ξ and η, the recursive formula for which can be found in Refs [24-27]. Using the DQEM rules (17)-(20), the eigenvalue Eqs. (13)-(14) can be discretized for element n into:

$$\frac{C_a^n}{\left(L_x^n\right)^2}\sum_{k=1}^{N_x}A_{ik}^{(2)}u_{kj}^n+\frac{C_b^n+C_c^n}{L_x^n L_y^n}\sum_{k=1}^{N_x}A_{ik}^{(1)}\sum_{m=1}^{N_y}\bar{A}_{jm}^{(1)}v_{km}^n+\frac{C_c^n}{\left(L_y^n\right)^2}\sum_{m=1}^{N_y}\bar{A}_{jm}^{(2)}u_{im}^n=-C_d^n\omega^2 u_{ij}^n \tag{21}$$

$$\frac{C_a^n}{\left(L_y^n\right)^2}\sum_{m=1}^{N_y}A_{jm}^{(2)}v_{im}^n+\frac{C_b^n+C_c^n}{L_x^n L_y^n}\sum_{k=1}^{N_x}A_{ik}^{(1)}\sum_{m=1}^{N_y}\bar{A}_{jm}^{(1)}u_{km}^n+\frac{C_c^n}{\left(L_x^n\right)^2}\sum_{k=1}^{N_x}A_{ik}^{(2)}v_{kj}^n=-C_d^n\omega^2 v_{ij}^n \tag{22}$$

where $i = 1, 2, \ldots, N_x$ and $j = 1, 2, \ldots, N_y$. The superscript n denotes the n-th element and $n = 1, 2, \ldots, 9$.

For the grid points at the four edges of element n, the corresponding boundary conditions described by Eqs. (10)-(11) and (15), or compatibility conditions (will be given in detail in Section 2.3) are used. Therefore, the element equilibrium equation in matrix form can be written as:

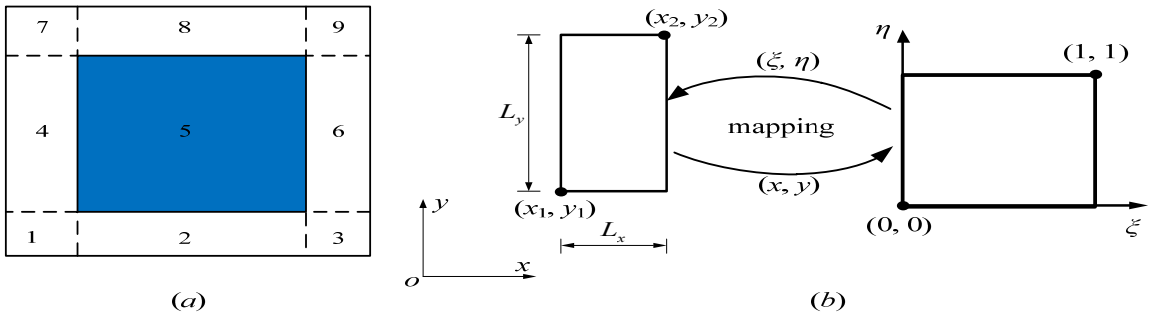

Fig. 3
(a) Illustration of the decomposition of the Wigner-Seitz cell, (b) Geometric transformation of an arbitrary rectangle onto a normalized square.

$$\mathbf{K}^n(k_x,k_y)\mathbf{d}^n = \omega^2\mathbf{M}^n\mathbf{d}^n \tag{23}$$

where $\mathbf{K}^n$, $\mathbf{d}^n$ and $\mathbf{M}^n$ are the element weighting coefficient matrix, the element displacement vector and the element consistent mass matrix, respectively. And

$$\mathbf{d}^n = [u_{11}^n, v_{11}^n, u_{12}^n, v_{12}^n, ..., u_{N_xN_y}^n, v_{N_xN_y}^n]^T \tag{24}$$

From the boundary conditions (10)-(11), we find that the matrix $\mathbf{K}^n$ is a function of the wave vector (k_x, k_y). The frequency can be determined if the value of wave vector (k_x, k_y) is specified. It is unnecessary to specify all values of (k_x, k_y). Actually, owing to the high symmetry of the structure, the band gaps can be obtained by changing the wave vector along the boundary of the first irreducible Brillouin zone, i.e., a triangle Γ-X-M in the reciprocal space [18, 28]. Herein Γ, X and M are three symmetry points $(0,0)$, $(\pi/l_{mx},0)$ and $(\pi/l_{mx}, \pi/l_{my})$, respectively.

2.3 Assembly of elements and compatibility conditions

By assembling the weighting coefficient matrices, the displacement vector and the mass matrices of all elements, the global system equations for all the nodal points of the plate labeled from 1 to N can be established as follows:

$$\mathbf{K}(k_x,k_y)\mathbf{d} = \omega^2\mathbf{M}\mathbf{d} \tag{25}$$

where $\mathbf{K}$, $\mathbf{d}$ and $\mathbf{M}$ are the overall weighting coefficient matrix, global displacement vector and overall mass matrix for the whole plate in the polar coordinates. And

$$\mathbf{d} = [u_1, v_1, u_2, v_2, ..., u_N, v_N]^T \tag{26}$$

The displacement compatibility and the equilibrium conditions should be satisfied at the interface boundaries of the plate. Obviously, the displacement compatibility conditions are automatically satisfied at all the interface conjunction nodes since the same global nodal number is used for each conjunction node. Only the equilibrium conditions are needed to form the compatibility conditions, which are built up as follows.

(1) Conjunction nodes at which two elements n_1 and n_2 meet.

For the case in which two elements are connected in the x-direction as shown in Fig. 4(a), the compatibility conditions are expressed as:

$$(T_x^{n_1})_{N_x,j} = (T_x^{n_2})_{1,j}, \quad (T_{xy}^{n_1})_{N_x,j} = (T_{xy}^{n_2})_{1,j} \tag{27}$$

For the case in which two elements are connected in the *y*-direction as shown in Fig. 4(b), the compatibility conditions are given as:

$$(T_y^{n_1})_{i,N_y} = (T_y^{n_2})_{i,1},\ (T_{xy}^{n_1})_{i,N_y} = (T_{xy}^{n_2})_{i,1} \tag{28}$$

(2) Conjunction nodes at which four elements meet.

If four adjacent elements n_1, n_2, n_3 and n_4 are connected at a node m as shown in Fig. 4(c), the compatibility conditions for the common node *m* can be expressed as:

$$(T_x^{n_1})_{N_x,N_y} + (T_x^{n_2})_{N_x,1} = (T_x^{n_3})_{1,1} + (T_x^{n_4})_{1,N_y},\ (T_{xy}^{n_1})_{N_x,N_y} + (T_{xy}^{n_2})_{N_x,1} = (T_{xy}^{n_3})_{1,1} + (T_{xy}^{n_4})_{1,N_y} \tag{29}$$

or

$$(T_y^{n_1})_{N_x,N_y} + (T_y^{n_4})_{1,N_y} = (T_y^{n_2})_{N_x,1} + (T_y^{n_3})_{1,1},\ (T_{xy}^{n_1})_{N_x,N_y} + (T_{xy}^{n_4})_{1,N_y} = (T_{xy}^{n_2})_{N_x,1} + (T_{xy}^{n_3})_{1,1} \tag{30}$$

(3) Conjunction nodes located at the boundaries of plate.

Take the left and right edges of the plate as an example for illustration. Suppose that the point m_1 and m_2 are two points on the left and right edges, respectively, with the same value of *y* coordination. The point m_1 is the conjunction node of elements n_1 and n_2 on the left boundary, and the point m_2 is the conjunction node of elements n_3 and n_4 on the right boundary. Besides two periodic displacement boundary conditions $u_{m_2} = u_{m_1} e^{ik_x l_{mx}}$ and $v_{m_2} = v_{m_1} e^{ik_x l_{mx}}$, the periodic boundary conditions for stress resultants at the points m_1 and m_2 can be expressed as:

$$(T_x^{n_3})_{N_x,j} + (T_x^{n_4})_{N_x,j} = [(T_x^{n_1})_{1,j} + (T_x^{n_2})_{1,j}]e^{ik_x l_{mx}},\ (T_{xy}^{n_3})_{N_x,j} + (T_{xy}^{n_4})_{N_x,j} = [(T_{xy}^{n_1})_{1,j} + (T_{xy}^{n_2})_{1,j}]e^{ik_x l_{mx}} \tag{31}$$

The periodic boundary conditions for bottom and top edges of the plate can be obtained in a similar way.

3 BAND GAPS IN PERIODIC PLATES

The validation of the DQEM are conducted firstly. Parametric studies are then undertaken to investigate the influences of the physical and geometrical parameters on the band gaps. In what follows, we take the sampling points for all elements as $N^e = N_x = N_y$. Comparisons of the numerical results with a varying number of sampling points N^e used in the DQEM approximation indicate that the present method converges well enough to produce convergent results when $N^e \geq 9$. In what follows, therefore, the number of the sampling points will be taken as N^e=9. Unless otherwise stated, the lattice constants $l_m = l_{mx} = l_{my}$ and the length of piezoelectric patch $l_p = l_{px} = l_{py}$.

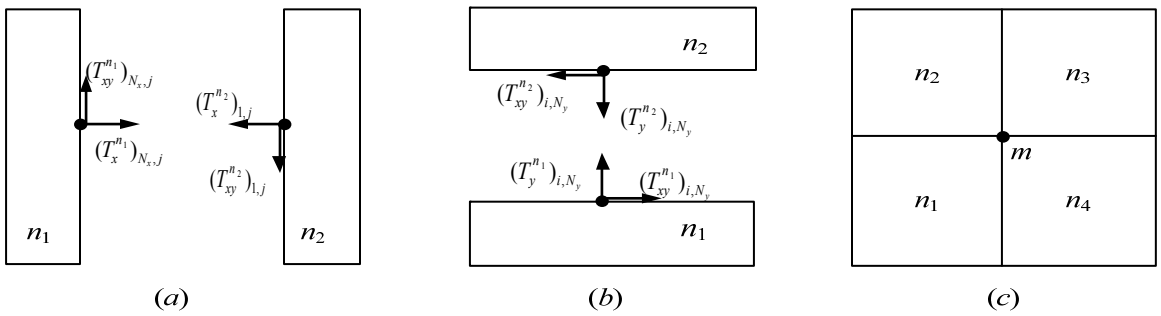

Fig. 4
Conjunction nodes on the interface boundaries of elements.

3.1 Validation

An infinite plate with piezoelectric patches bonded periodically is considered. The dimension of its Wigner-Seitz cell are that h_m=h_p=1.25 mm, l_m=77 mm and l_p=37 mm. The plate is aluminum of which the density is 2710 kg/m^3, the Young's modulus 69GPa and the Poisson ratio 0.33. The piezoelectric patch is BM500 of which the material coefficients are listed in Table 1. The coefficient S_d of BM500 is very small (1.9×10^{-12} m^2/N), so the difference between the results for open-circuit and closed-circuit conditions is not obvious, and we consider the case of open-circuit only in what follows.

To validate the present method, a three-dimensional (3D) finite element model (FEM) is built using the commercial software ANSYS. Both the piezoelectric patch and the elastic plate are modeled by the element SOLID5. The periodic boundary conditions (10)-(11) are applied using the method introduced by Åberg and Gudmundson [29]. The in-plane band structure (dispersion curves) of the periodic plate by present method and FEM are compared in Fig.5. Excellent agreement can be observed in the first branch for shear waves. The results obtained by FEM are slight higher than that by DQEM in the second branch for the compression waves. It is worth to mention that the group velocity of waves, i.e., the slope of curves shown in Fig.5, should be zero at the high symmetric point X [28]. The velocity predicted by DQEM always obeys this law, which indicates that the present method is reliable.

There is a frequency band gap as shown in Fig.5. The band gaps obtained by FEM and DQEM are 24.81 kHz-30 kHz and 25.00 kHz-29.92 kHz, respectively, which are almost identical. For the plate, the upper bound frequency and the lower bound frequency of the band gap can be obtained at point A and point B, respectively.

Table 1
Materials coefficients of BM500 ($\in_0 = 8.85\times10^{-12}\,\mathrm{F/m^2}$)

Density (kg/m^3)	Elastic compliance(10^{-12}m^2/N)						Piezoelectric (10^{-12}C/N)			Dielectric ($\times\in_0$)	
ρ	S_{11}	S_{12}	S_{13}	S_{33}	S_{44}	S_{66}	d_{31}	d_{15}	d_{33}	$\in_{11}$	$\in_{33}$
7650	16.26	-5.67	-7.17	18.72	47.39	44.25	-170.4	582.9	373.2	1726	1704

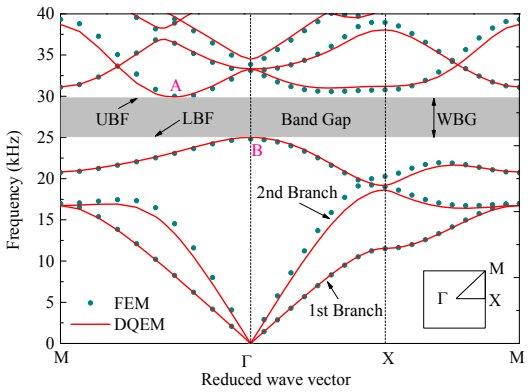

Fig. 5
Band structure of a square-lattice two-dimensional infinite piezoelectric plate. Inset shows the irreducible part of the irreducible Brillouin zone.

3.2 Parameter studies

In this section, parametric studies are conducted to investigate the influences of the geometrical and physical parameters on the lower bound frequency (LBF), the upper bound frequency (UBF) and the width of the band gap (WBG). Unless otherwise stated, the units size l_m = 77 mm and the thickness of the hosted plate is h_m = 1.25 mm in what follows.

First of all, we investigate the effect of geometrical parameters on the band gap. Two geometrical parameters are considered: the length ratio $\alpha = l_p / l_m$ and the thickness ratio $\beta = h_p / h_m$. The size of the elastic plate is kept constant but the dimension of the piezoelectric patch is varied such that the two ratios are changed. Fig. 6

investigates the influence of the length ratio on the band gap. The numerical results show that the band gap will disappear when the length ratio α is out of the range (0.362, 0.848). Actually, a very small length ratio means that the effect of the piezoelectric patch can be neglected. In other words, the structure can be considered as an elastic plate if α is closed to zero. On the other hand, when the ratio is closed to one, the piezoelectric patch will tend to cover the whole cell, and then the structure can be considered a multilayered composite plate. Both cases weak the periodicity of the structure and the band gap will not exist. Both the LBF and UBF decreases monotonically as the ratio α increases. The peak value of WBG is found at $\alpha = 0.55$. Fig. 7 shows the effect of the thickness ratio β on the band gap. Again, the band gap will disappear when $\beta < 0.51$. The periodicity of the structure is not obvious when the ratio become smaller and smaller. On the other side, when the ratio becomes larger and larger, the WBG will be wider and wider, i.e., the periodicity is more significant. We also find that the UBF remains almost a constant at 30 kHz and the LBF decreases as the ratio varied from 0.51 to 2.5. In order to understand the physical insight of this phenomenon, we calculate the modulus of the complex displacement field of the modes at points A and B (see Fig. 5), at which the modes are corresponding to the UBF and LBF, respectively. The displacement modulus for these two modes are shown in Fig.8. For the point A, the displacement in the four corners of the cell is very large. However, the displacement is very small in the area within the piezoelectric patch. In other words, this mode is highly dependent on the elastic plate instead of the piezoelectric patch. Therefore, the thickness ratio have no effect on the UBF when the thickness of the patch is increased and the thickness of the elastic plate is kept as a constant. For the point B, we find a different map that the displacement has its largest magnitude in the most part of the patch and it is almost zero near the edges of the cell. We can characterize qualitatively the vibration of the patch as a mass-spring oscillator. As the thickness of the patch increases, the total mass is increased and then the frequency will be decreased.

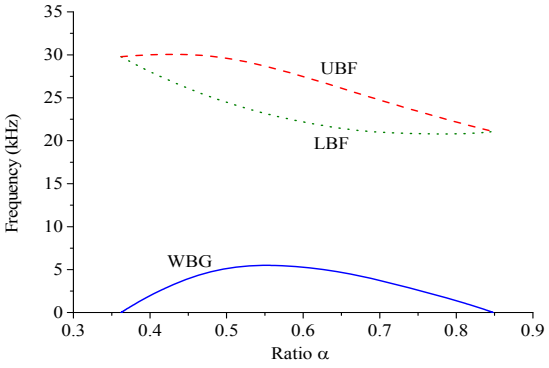

Fig. 6
Effect of the length ratio α on the band gap.

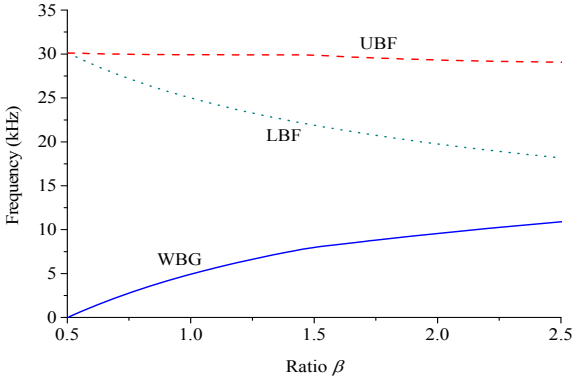

Fig. 7
Effect of the thickness ratio β on the band gap.

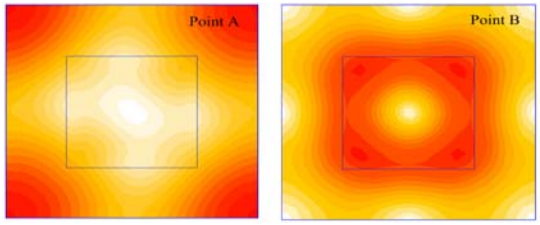

Fig. 8
The modulus of complex displacement field of the modes at points A (UBF) and B (LBF).

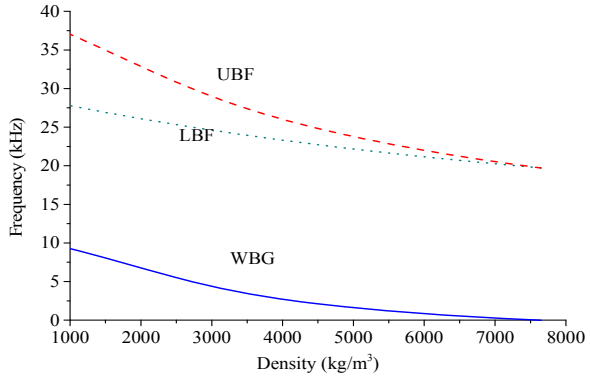

Fig. 9
Effect of density of the plate on the band gap.

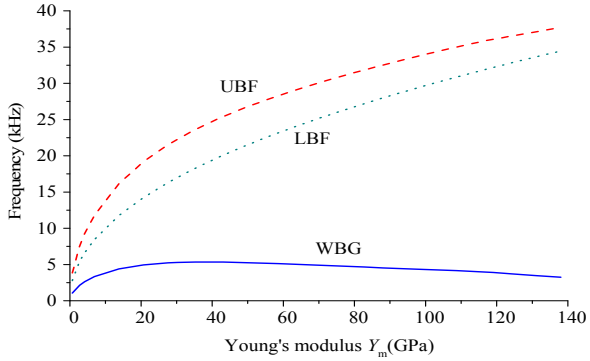

Fig. 10
Effect of Young's modulus of the plate on the band gap.

Next, we are dealing with the effect of physical parameters, i.e., the density and Young's modulus of the elastic plate, on the band gap. On one side, the increasing of the density ρ_m results in the increasing total mass of the system, so the LBF and UBF are decreased as shown in Fig.9. The WBG is also decreased and then vanishes as the density ρ_m varied from 1000 kg/m^3 to 7640 kg/m^3. Actually, the density of the piezoelectric patch is 7650 kg/m^3. That is to say that the band gap vanishes when the densities of the two materials are closer and closer. It also indicates that the density difference between two materials plays a very important role to form the band gap. On the other side, as shown in Fig. 10, increasing of the modulus of the plate Y_m, which means increasing the total stiffness of the system, leads to increasing of both LBF and UBF. However, the band width is not changed monotonically as the modulus Y_m varied. Its peak can be obtained at Y_m = 30GPa.

4 DYNAMIC RESPONSE OF PERIODIC PLATES

In the previous sections, we focus on infinite periodic piezoelectric plate and its band gap. However, all engineering structures are finite dimensional, so further study on the dynamic of finite dimensional quasi-periodic plates is very important. For practical purpose, we will investigate two periodic piezoelectric plates, A and B, as shown in Fig.11,

with finite dimension of length 307 mm and width 230 mm. The two plates differ in that all piezoelectric patches in plate A have dimension of 25 mm × 25 mm × 0.5 mm, whereas in plate B the dimension is 37 mm × 37 mm × 1.25 mm. The plate A was designed by Yaman, Çalışkan [30]. The plate B is the same as the plate discussed in section 3.1 but with finite dimension. Numerical simulations using ANSYS are conducted to highlight the effect of band gaps on the harmonic response and the transient response of the plates.

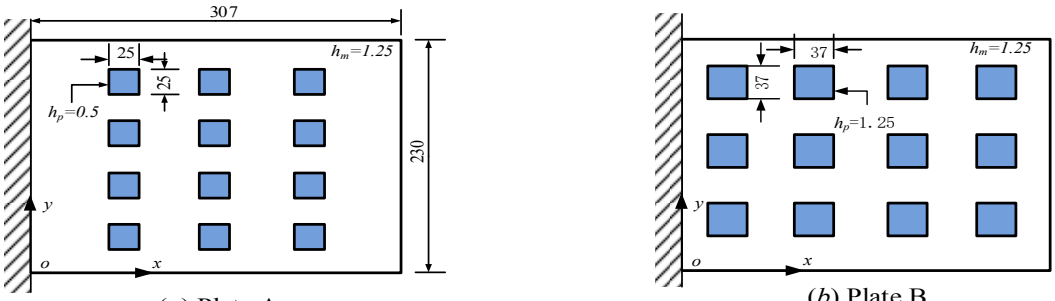

Fig. 11
Schematic diagram of two piezoelectric quasi-periodic plates (Unit: mm).

4.1 Harmonic analysis

Both plates are subjected to a harmonic dynamic base displacement at the clamed end $x = 0$. The harmonic dynamic base displacement is taken as $u = u_0 \sin(2\pi f \cdot t)$ where u_0 is its amplitude and f is the imposed frequency. The average tip displacement amplitude u_{tip} at all nodes of the free end is calculated by ANSYS. The transmitting frequency response functions (FRFs) is used to represent the dynamic character of the finite periodic plates. The FRFs is defined as $20\log(u_{tip}/u_0)$. Note that the value of FRFs will be zero if the displacement u_0 and the tip displacement u_{tip} are the same, and a negative value of FRFs indicates an effective reduction. The right parts of Figs.12 and 13 plot the frequency response function of plates A and B, respectively. If the plates are extended to infinite, we can calculate their band structures. For comparison, the band structures of the corresponding infinite plates are depicted in the left parts of the figures. Obviously, as shown in Fig.12(a), no band gap can be found in the considered frequency region (0-36.2 kHz). Therefore, there is no vibration attenuation as shown in Fig.12(b). As shown in Fig.13, it is found that the tip displacement of plate B is strongly reduced when the frequency of base excitation falls into the attenuation range (23.21 Hz, 27.82 Hz), which is closed to the band gap (25.00 Hz, 29.92 Hz). The finite quasi-periodic plate is consisted of only four cells in the x-direction, so the attenuation range is not totally match with the band gap. The attenuation range will be closed to the band gap if more periodic cells are considered.

4.2 Transient analysis

A dynamic base displacement is applied at the clamed end of the two quasi-periodic plates and a homogenous aluminum plate (307 mm × 230 mm × 1.25 mm). A general base excitation can be expanded in a sine series

$$u(t) = \sum_{n=1}^{N} u_n \sin(2\pi f_n t) \tag{32}$$

where *N* is the number of frequency components, u_n are the displacement amplitude of the *n*-th component f_n. For simplicity, the base excitation is considered as two harmonic vibrations of f_1 = 25 kHz, f_2 =28 kHz, u_1 =1 mm and u_2 =1 mm in this numerical example. Both frequencies are closed to the attenuation range (23.21 Hz, 27.82 Hz) of the plate *B* and fall into its band gap (25.00 Hz, 29.92 Hz). The time history of average displacement response of all

nodes at the free end are compared in Fig.14. As discussed previously, we can't get a band gap of which frequency is below 36.2 kHz in the plate A. Of course, there are no band gaps in the humongous plate too. As expected, the displacement response of the plate *B* is much less than that of other two plates.

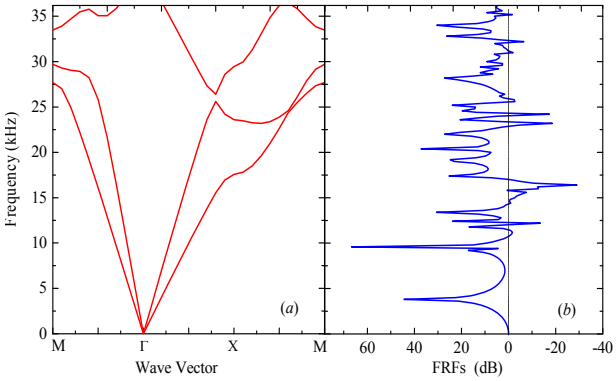

Fig.12
(a) Band structure; (b) Displacement response function for the plate of type A.

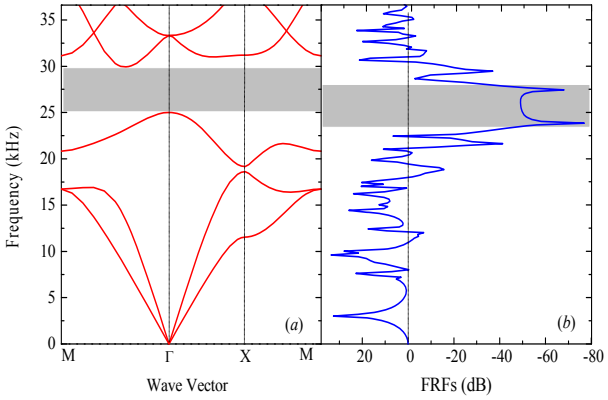

Fig. 13
(a) Band structure; (b) displacement response function for the plate of type B.

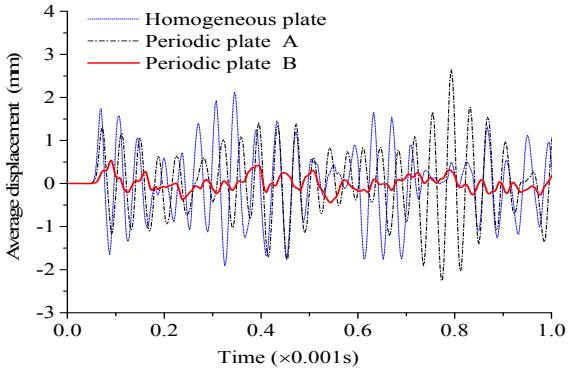

Fig. 14
Time history of average displacement of nodes at the free end.

5 CONCLUSIONS

A plate bonded periodically with piezoelectric patches is investigated in this work. Some conclusions can be given as follows

1. With introducing the periodic boundary conditions, we use the differential quadrature element method to analyze the band gaps in periodic piezoelectric plates. The method is simple and accurate and relative less sampling points are required.
2. The physical and geometrical parameters play an important role on the band gap. The effect of the length ratio on the band gap is very obvious. The maximum band width can be obtained by reasonably changing the ratio. However, the variation of thickness ratio only changes the LBF and has no effect on the UBF. The larger the thickness ratio is designed, the larger the band width is obtained. Increasing the density of the plate will enlarge both LBF and UBF, but a high value of Young's modulus of the plate will reduce the LBF and UBF of the band gap.
3. The attenuation of vibration response of the periodic plate may exceed 40dB if the excitation frequency falls into the band gap of the considered plate. Transient analysis also shows that a plate with band gap can reduce its dynamic response. This gives a new idea in structural design for the purpose of vibration control.

ACKNOWLEDGMENTS

This work is supported by the National Natural Science Foundation of China (51178040 and 51072018) and the Fundamental Research Funds for the Central Universities (2013JBM010).

APPENDIX A

For the area covered a piezoelectric patch:

$$C_a = \frac{2h_pY_p}{1-(\mu_p)^2} + \frac{h_mY_m}{1-(\mu_m)^2}, C_b = \frac{2h_p\mu_pY_p}{1-(\mu_p)^2} + \frac{h_m\mu_mY_m}{1-(\mu_m)^2}, C_c = 2h_pG_p + h_mG_m, C_d = 2\rho_ph_p + \rho_mh_m.$$

For the area without piezoelectric patch:

$$C_a = \frac{h_mY_m}{1-(\mu_m)^2}, C_b = \frac{h_m\mu_mY_m}{1-(\mu_m)^2}, C_c = h_mG_m, C_d = \rho_mh_m.$$

REFERENCES

[1] Sigalas M., Kushwaha M.S., Economou E.N., Kafesaki M., Psarobas I.E., Steurer W., 2005, Classical vibrational modes in phononic lattices: theory and experiment, *Zeitschrift für Kristallographie* **220**:765-809.

[2] Baz A., 2001, Active control of periodic structures, *Journal of Vibration and Acoustic* **123**: 472-479.

[3] Kushwaha M.S., Halevi P., Dobrzynski L., Djafari-Rouhani B., 1993, Acoustic band structure of periodic elastic composites, *Physical Review Letters* **71**(13): 2022-2025.

[4] Kushwaha M.S., Halevi P., 1994, Band gap engineering in periodic elastic composites, *Applied Physics Letters* **64**(9): 1085-1087.

[5] Liu Z., Zhang X., Mao Y., Zhu Y.Y., Yang Z., Chan C.T., Sheng P., 2000, Locally resonant sonic materials, *Science* **289**(5485): 1734-1736.

[6] Jia G., Shi Z., 2010, A new seismic isolation system and its feasibility study, *Earthquake Engineering and Engineering Vibration* **9**(1): 75-82.

[7] Bao J., Shi Z.F., Xiang H.J., 2012, Dynamic responses of a structure with periodic foundations, *Journal of Engineering Mechanics-ASCE* **138**(7): 761-769.

[8] Xiang H.J., Shi Z.F., Wang S.J., Mo Y.L., 2012, Periodic materials-based vibration attenuation in layered foundations: experimental validation, *Smart Materials and Structures* **21**(11): 112003.

[9] Xiong C., Shi Z.F., Xiang H.J., 2012, Attenuation of building vibration using periodic foundations, *Advances in Structural Engineering* **15**(8): 1375-1388.

[10] Khelif A., Djafari-Rouhani B., Vasseur J.O., Deymier P.A., Lambin P., Dobrzynski L., 2002, Transmittivity through straight and stublike waveguides in a two-dimensional phononic crystal, *Physical Review B* **65**(17): 174308.

[11] Khelif A., Aoubiza B., Mohammadi S., Adibi A., Laude V., 2006, Complete band gaps in two-dimensional phononic crystal slabs, *Physical Review E* **74**(4): 046610.

[12] Thorp O., Ruzzene M., Baz A., 2001, Attenuation and localization of wave propagation in rods with periodic shunted piezoelectric patches, *Smart Materials and Structures* **10**: 979.
[13] Wang Y.Z., Li F.M., Kishimoto K., Wang Y.S., Huang W.H., 2009, Wave band gaps in three-dimensional periodic piezoelectric structures, *Mechanics Research Communications* **36**(4): 461-468.
[14] Wu T.T., Hsu Z.C., Huang Z.G., 2005, Band gaps and the electromechanical coupling coefficient of a surface acoustic wave in a two-dimensional piezoelectric phononic crystal, *Physical Review B* **71**(6): 064303.
[15] Zou X.Y., Chen Q., Liang B., Cheng J.C., 2008, Control of the elastic wave bandgaps in two-dimensional piezoelectric periodic structures, *Smart Materials and Structures* **17**: 015008.
[16] Xiang H.J., Shi Z.F., 2009, Analysis of flexural vibration band gaps in periodic beams using differential quadrature method, *Computers & Structures* **87**(23-24): 1559-1566.
[17] Xiang H.J., Shi Z.F., 2011, Vibration attenuation in periodic composite Timoshenko beams on Pasternak foundation, *Structural Engineering and Mechanics* **40**(3): 373-392.
[18] Kittel C., 2005, Introduction to Solid State Physics, John Wiley & Son, New York, 8th Edition.
[19] Chen C.N., 2004, Extended GDQ and related discrete element analysis methods for transient analyses of continuum mechanics problems, *Computers & Mathematics with Applications* **47**(1): 91-99.
[20] Chen C.N., 2008, DQEM analysis of out-of-plane vibration of nonprismatic curved beam structures considering the effect of shear deformation, *Advances in Engineering Software* **39**(6): 466-472.
[21] Malekzadeh P., Karami G., Farid M., 2004, A semi-analytical DQEM for free vibration analysis of thick plates with two opposite edges simply supported, *Computer Methods in Applied Mechanics and Engineering* **193**(45-47): 4781-4796.
[22] Liu F.L., Liew K.M., 1999, Differential quadrature element method: a new approach for free vibration analysis of polar Mindlin plates having discontinuities, *Computer Methods in Applied Mechanics and Engineering* **179**(3): 407-423.
[23] Eisinberg A., Fedele G., 2005, Vandermonde systems on gauss-lobatto chebyshev nodes, *Applied Mathematics and Computation* **170**(1): 633-647.
[24] Shu C., 2000, *Differential Quadrature: And Its Application in Engineering*, Springer, London.
[25] Shu C., Richards B.E., 1992, Application of generalized differential quadrature to solve two-dimensional incompressible Navier-Stokes equations, *International Journal for Numerical Methods in Fluids* **15**(7): 791-798.
[26] Xiang H.J., Yang J., 2008, Free and forced vibration of a laminated FGM timoshenko beam of variable thickness under heat conduction, *Composites Part B-Engineering* **39**(2): 292-303.
[27] Yang J., Xiang H.J., 2007, Thermo-electro-mechanical characteristics of functionally graded piezoelectric actuators, *Smart Materials and Structures* **16**(3): 784-797.
[28] Wen X.S., Wen J.H., Yu D.L., Wang G., Liu Y.Z., Han X.Y., 2009, *Phononic Crystals*, Ational Defense Industry Press, Beijing.
[29] Åberg M., Gudmundson P., 1997, The usage of standard finite element codes for computation of dispersion relations in materials with periodic microstructure, *The Journal of the Acoustical Society of America* **102**(4): 2007-2013.
[30] Yaman Y., Çalışkan T., Nalbantoğlu V., Prasad E., Waechter D., 2002, *Active Vibration Control of a Smart Plate,* ICAS2002, Toronto, Canada.